

# $^4\text{He}$ adsorbed inside (10,10) single walled carbon nanotubes

M.C.Gordillo

*Departamento de Sistemas Físicos, Químicos y Naturales. Facultad de Ciencias Experimentales.  
Universidad Pablo de Olavide. Carretera de Utrera, km 1. 41013 Sevilla. Spain.*

J. Boronat and J. Casulleras

*Departament de Física i Enginyeria Nuclear, Universitat Politècnica de Catalunya,  
B4-B5 Campus Nord. 08034 Barcelona. Spain.*

(Dated: November 20, 2018)

Diffusion Monte Carlo calculations on the adsorption of  $^4\text{He}$  in open-ended single walled (10,10) nanotubes are presented. We have found a first order phase transition separating a low density liquid phase in which all  $^4\text{He}$  atoms are adsorbed close to the tube wall and a high density arrangement characterized by two helium concentric layers. The energy correction due to the presence of neighboring tubes in a bundle has also been calculated, finding it negligible in the density range considered.

PACS numbers: 68.90.+g,05.30.-d

One of the most interesting capabilities of carbon nanotubes and their bundles is their purported use as reservoirs, in particular for the lightest quantum fluids ( $^4\text{He}$ ,  $\text{H}_2$  and  $\text{Ne}$ )<sup>1,2,3,4,5,6</sup>. The most obvious adsorption places are the outer part of the bundles, formed by the depressions known as grooves between every two tubes, and the rest of the exposed external surfaces. These adsorption places have already been experimentally documented<sup>3,6,7,8</sup>. One can think also of the interchannels located every three – or more if the arrangement is irregular – tubes in the inner part of the bundle as accessible sites, but this latter possibility seems uncertain since any single vacancy in the carbon structure of the nanotubes could block those very thin interstices<sup>9</sup>.

The other possible adsorption site is the inner part of the tubes themselves. This would imply to remove the ending caps of the nanotubes and thus allowing the gases to enter. To our knowledge, there is no experimental information for this last possibility in the case of  $^4\text{He}$ , the majority of theoretical studies being related to the limit of infinite dilution<sup>10</sup> or to quasi one-dimensional narrow environments<sup>11,13,14</sup>, even though there are some exceptions<sup>15,16,17</sup>. In the present work, we present a study of  $^4\text{He}$  adsorbed in a (10,10) single walled carbon nanotube, one of the most common types. We have also estimated the effect that neighboring tubes have in the adsorption energies of  $^4\text{He}$  inside a single tube. That can help to make a good estimation of the real adsorption capabilities of nanotube bundles.

We have carried out a microscopic study of the system at zero temperature using the Diffusion Monte Carlo (DMC) method. DMC is a stochastic technique for solving the many-body Schrödinger equation, providing for boson systems exact results within some statistical uncertainties<sup>18</sup>. The carbon atoms in the nanotubes have been explicitly considered, meaning that the carbon nanotube-helium potential was obtained by summing up all the C-He pair interactions (taken from Ref. 19), with the carbon atoms in fixed positions. This is not the most

common setup, since most of the previous studies were carried out considering a smoothed helium-tube interaction (an exception being Ref. 15). The helium-helium potential is the HFD-B(HE) Aziz potential<sup>20</sup>. For the liquid phase simulations (see below), we have used  $N = 150$   $^4\text{He}$  atoms, and to run calculations at different densities we have changed the length of the simulation cell between 1537.5 and 34.44 Å, these values being in all cases a multiple of the elementary carbon cell of length 2.46 Å, characteristic of an armchair nanotube. When a solid-liquid system was considered, we fixed the number of atoms belonging to the solid phase, and varied the number of atoms in the liquid one. Periodic boundary conditions in the transverse direction ( $z$  in cylindrical coordinates) have always been assumed.

The trial wave function needed in the method for guiding the diffusion process was chosen to be of the form:

$$\Psi(\mathbf{r}_1, \dots, \mathbf{r}_N) = \prod_{i < j}^N f_{\text{He-He}}(r_{ij}) \prod_{i,j=1}^{N,N_c} f_{\text{He-C}}(r_{ij}) \prod_{i=1}^N \Phi(r_i), \quad (1)$$

with  $N$  and  $N_c$  the number of  $^4\text{He}$  and C atoms, respectively, and  $r_i$  the radial distance of particle  $i$  to the center of the nanotube. The first two terms of  $\Psi$  in Eq. (1) correspond to two-body correlation factors which account for dynamical correlations induced by the He-He and He-C potentials. Both  $f_{\text{He-He}}(r)$  and  $f_{\text{He-C}}(r)$  are of McMillan type,  $f(r) = \exp[-0.5(b/r)^5]$ . The value for the parameters  $b_{\text{He-He}}$  has been taken from Ref. 18. The value of  $b_{\text{C-He}}$  varied from the phases with one helium layer ( $b_{\text{He-He}} = 0$ ) to the ones with two helium layers ( $b_{\text{He-He}} = 2.3$  Å, see below). In both cases,  $b$  was obtained by means of separate Variational Monte Carlo (VMC) calculations and found to be independent on the helium density.

The variance of the calculation is reduced by introducing also in the trial wave function (1) a one-body term  $\Phi(r_i)$  which accounts for the mean interaction between a single He atom and the nanotube wall. At small densities,

we have taken for  $\Phi(r_i)$  the solution of the Schrödinger equation for a single  $^4\text{He}$  atom in the cylindrically averaged potential of Ref. 19 for a tube of the same diameter than a (10,10) one. This function has a single peak located roughly in the minimum of the considered helium-tube potential. When the density increases one can see the emergence of a second peak in the density profile obtained from the DMC simulations. This peak is located nearer to the center of the nanotube than the previous one. Thus, in the high density regime we verified that the variance is further reduced by changing the low-density one-body term to another one which contains this closer-to-the-center peak in addition to the one near the carbon wall. In particular, we have used for  $\Phi(r_i)$  the square root of the radial density profile obtained in a DMC calculation at density  $\rho = 0.028 \text{ \AA}^{-3}$ . This trial wave function has two maxima and a reduced density (but not zero) between them. In principle, this profile with the double peak would correspond to a liquid phase since no localization on fixed sites of any of the helium atoms was imposed.

When the density increases even more the layer closer to the wall can crystallize. In order to characterize this possible solid layer we have also studied the system by introducing Nosanow-Jastrow terms describing a solid order around the cylinder,

$$\Psi_s(\mathbf{r}_1, \dots, \mathbf{r}_N) = \prod_{i=1}^{N_s} g(|\mathbf{r}_i - \mathbf{R}_i|) \Psi(\mathbf{r}_1, \dots, \mathbf{r}_N), \quad (2)$$

with  $\Psi$  the trial wave function of the liquid phase with a double peak (1) and  $g(r)$  a gaussian factor localizing a given set of particles around predefined lattice sites  $\mathbf{R}_i$ . The lattice chosen for the simulation corresponds to a triangular-like planar lattice rolled up to form a cylinder concentric to the carbon nanotube. A VMC optimization process was performed first by using a fixed number of atoms (150) for different lengths of the simulation cell, and varying also the number of atoms located in the first and second helium layers. We then compared the simulation results to those without the gaussian constrains at the same density. Those set of optimizations led us to conclude that the minimum energy configurations in the density range studied correspond to a lattice formed by slices of eight atoms that approximately share the same  $z$  coordinate (that of the tube axis) and are separated by a distance of  $2.46 \text{ \AA}$  in the  $z$  direction. This layer is located at a distance of  $2.8 \text{ \AA}$  from the carbon wall. Any other 2D solid phases, including registered ones we found to produce configurations of higher energy. In the final simulations, we have used 14 nanotube cells that, with this optimized structure, represent a solid layer composed by 112  $^4\text{He}$  atoms. The rest of the helium, up to 150 atoms, was considered to be in the second layer and was disposed without gaussian restrictions. The free parameter of the gaussian  $g(r) = \exp(-\alpha r^2)$  has been optimized ( $\alpha=2.30 \text{ \AA}^{-2}$ ) showing negligible dependence on the density in the range studied. A check was also made to see the influence of the corrugation imposed by the carbon structure

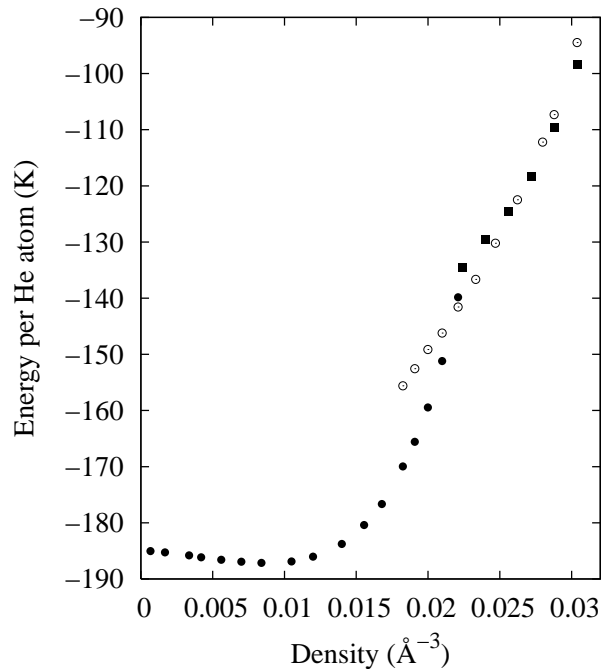


FIG. 1: Energy versus density for different elections of the trial function: One layer liquid (full circles); (squares); two layer liquid (circles); a close to the wall solid (full squares).

in the energy of the solid layer. To do so, we located the solid lattice in different positions relative to the underlying structure. The energies obtained were similar within the error bars, what indicates that the solid layer is a two-dimensional incommensurate solid.

The results for the total set of simulations of  $^4\text{He}$  inside a single (10,10) tube are displayed in Fig. 1. The densities were calculated by straightforwardly dividing the number of atoms by the nanotube volume, considering a radius of  $6.8 \text{ \AA}$  in all cases. Full circles are the results for a one-layer He phase, open circles correspond to the two-layer liquid arrangement, and the full squares indicate the energies obtained for the phase with a solid layer closer to the carbon wall. The main conclusion one can draw from this figure is that there is a minimum of energy of the one-shell phase; corresponding to zero pressure and that can be found from a third order polynomial fit to be at  $0.0086 \text{ \AA}^{-3}$  with a corresponding binding energy of  $187.18 \pm 0.02 \text{ K}$ . The same binding energy for the infinite dilution limit is  $185.01 \pm 0.02 \text{ K}$ . That is bigger than the experimental value for graphite,  $143 \pm 2 \text{ K}$ <sup>25</sup>, and smaller than the corresponding values for a (5,5) tube ( $429.984$  and  $429.966 \text{ K}$  at zero pressure and for infinite dilution, respectively). This simply means that an increasing in the tube radius implies a lowering of the binding energy to approximate the one in the flat surface of graphite. What is more important, the stable phase at zero pressure and  $0 \text{ K}$  is a *liquid*. In this respect, the situation is different than in the case of graphite<sup>23</sup> and for the cylindrical system considered in Ref. 16.

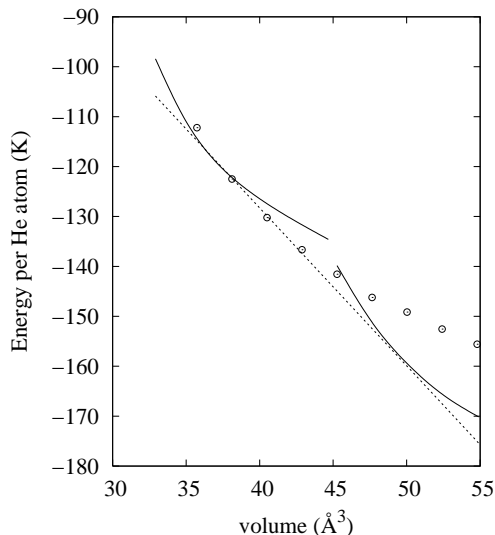


FIG. 2: Maxwell construction to determine the stability range of the phases involved in the modeling of the system. Full line, one layer liquid and solid+liquid phases ; Circles, two layer liquid phase.

The stability of the rest of the phases can be deduced with the help of Fig. 2. This is a Maxwell construction for the density range in which we could have a two-layer liquid or a two-layer solid+liquid. Full lines are third-grade polynomial fits to the corresponding one layer liquid phase, and the two-layer solid+liquid arrangement, while circles are the results for the two-layer liquid. The x axis corresponds to the inverse of the density as defined in the previous figure. The dashed line is a double tangent construction between the one-layer liquid and the phase including a solid. In a conservative frame, this would indicate a transition between a low density phase of  $2 \cdot 10^{-2} \text{ \AA}^{-3}$  and a one including a solid, of  $2.7 \cdot 10^{-2} \text{ \AA}^{-3}$ . The transition pressure would be of 430 atm. However, another alternative explanation can be deduced from the data, and it is a double transition between a single layer liquid and a double layer liquid, followed by another one between this last dense liquid and the solid and liquid phase. The corresponding coexistence densities are the same for the two phases already mentioned, but we will have small a window with a two-layer liquid at around  $2.5 \cdot 10^{-2} \text{ \AA}^{-3}$ . The one shell liquid- two shell liquid transition would be then at 420 atm. Unfortunately, the available data (and shown in Table I) will not allow us to discriminate between both scenarios. In any case, it is clear that an increasing in the density will eventually create a solid close to the wall.

To complete the characterization of the phases, we displayed the radial profiles for different helium densities in Fig. 3. The dashed line represents the case of zero pressure ( $0.0086 \text{ \AA}^{-3}$ ), while the dotted line displays the situation in the low density limit of the transition region. One can see that in both cases the system is formed by a single cylindrical helium shell, located at around 4 Å from

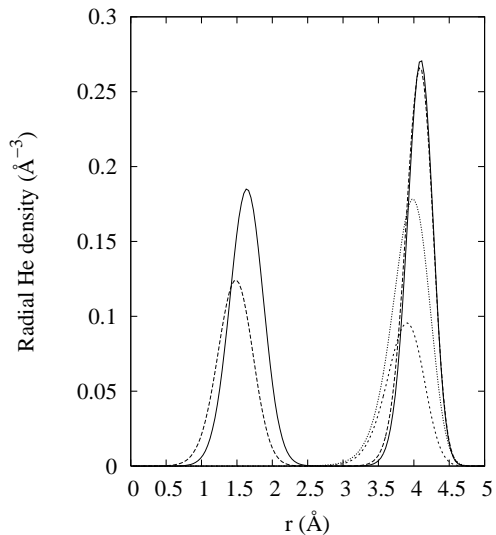


FIG. 3: Radial density profiles at zero pressure (dashed line), at the lower and upper limits of the coexistence regions (dotted and long dashed line, respectively). The solid line represents the case for the solid+liquid phase at the highest density simulated.

the center of the tube. The main difference is the increasing in the helium density that can be inferred from the growth in the corresponding peak. The long-dashed line indicates the situation in the upper density limit of the coexistence zone for the case of the solid+liquid phase. We observe a second peak located closer to the center of the tube, and another one corresponding to the two-dimensional solid, roughly in the same position than in the single layer phase. Finally, the full line represents the solid+liquid phase at the highest density simulated. There, the first peak is virtually identical to the one at the transition, as befits to a solid of unchanging density, going the additional helium to fill the second layer.

Until now, we considered only the case of an isolated carbon nanotube, but this is not the most common situation, since those cylinders tend to group to form what is termed a bundle. There, each tube is ideally surrounded by six others, forming a structure whose section is similar to a triangular 2D lattice with a minimum distance between centers of cylinders of  $17 \text{ \AA}^{22}$ . Taking that into account, we estimated the influence that the surrounding tubes have in the energy per helium atom within a mean field scheme by means of the following expression:

$$E_{correction} = 6 \int_{x'} \int_{y'} d(x', y') dx' dy' \quad (3)$$

$$\times \int_0^\infty \int_x \int_y R(x, y, z) V(x, y, z, x', y') dx dy dz$$

where  $d(x', y')$  represents the normalized probability of finding an  $^4\text{He}$  atom at coordinates  $x'$  and  $y'$  for any  $z$  position in the first tube.  $R(x, y, z)$  is the corresponding radial density function as the ones depicted in Fig. 3,

TABLE I: Energies per  $^4\text{He}$  atom in K at several densities.

Density ( $\text{\AA}^{-3}$ )	(10,10) tube	$E_{\text{correction}}$
Low density phase		
$6.7 \cdot 10^{-4}$	-185.02(4)	-0.003
$1.7 \cdot 10^{-3}$	-185.27(3)	-0.006
$3.4 \cdot 10^{-2}$	-185.81(3)	-0.013
$4.2 \cdot 10^{-3}$	-186.14(4)	-0.016
$5.6 \cdot 10^{-3}$	-186.58(3)	-0.022
$7.0 \cdot 10^{-3}$	-186.93(4)	-0.027
$8.4 \cdot 10^{-3}$	-187.14(3)	-0.033
$1.05 \cdot 10^{-2}$	-186.89(3)	-0.041
$1.2 \cdot 10^{-2}$	-186.02(4)	-0.047
$1.4 \cdot 10^{-2}$	-183.76(4)	-0.055
$1.6 \cdot 10^{-2}$	-180.40(4)	-0.062
$1.7 \cdot 10^{-2}$	-176.66(4)	-0.067
$1.8 \cdot 10^{-2}$	-169.97(4)	-0.073
$1.9 \cdot 10^{-2}$	-165.59(6)	-0.077
$2.0 \cdot 10^{-2}$	-159.45(7)	-0.081
Two layer liquid density phase		
$1.8 \cdot 10^{-2}$	-155.60(9)	-0.069
$1.9 \cdot 10^{-2}$	-152.56(9)	-0.072
$2.0 \cdot 10^{-2}$	-149.15(7)	-0.075
$2.1 \cdot 10^{-2}$	-146.22(9)	-0.079
$2.2 \cdot 10^{-2}$	-141.58(6)	-0.083
$2.3 \cdot 10^{-2}$	-136.66(6)	-0.087
$2.5 \cdot 10^{-2}$	-130.22(8)	-0.092
$2.6 \cdot 10^{-2}$	-122.49(8)	-0.099
$2.8 \cdot 10^{-2}$	-112.2(1)	-0.103
Two layer liquid+solid density phase		
$2.2 \cdot 10^{-2}$	-134.58(5)	-0.092
$2.4 \cdot 10^{-2}$	-129.63(5)	-0.095
$2.6 \cdot 10^{-2}$	-124.50(5)	-0.099
$2.7 \cdot 10^{-2}$	-118.30(5)	-0.103
$2.9 \cdot 10^{-2}$	-109.64(6)	-0.107
$3.0 \cdot 10^{-2}$	-98.41(9)	-0.111

and depends on the location of helium atoms in the second tube  $(x, y, z)$ . Finally,  $V(x, y, z, x', y')$  is the helium-

helium Aziz potential used in our simulations<sup>20</sup>. The result of the integral is multiplied by six to take into account the number of tubes surrounding a particular one at the same distance. A check of the accuracy of this kind of mean field estimation has already been done for a closely related system<sup>24</sup> and found a very good approximation to the results of a full Monte Carlo calculation.

The results of this energy correction are given in Table I. One thing is immediately apparent, and it is that the mean field term increases with density, but in all cases is negligible and of the order of the error bars of the DMC calculation. That means that the binding energy of  $^4\text{He}$  in a bundle is essentially the same that the one for a single tube.

Summarizing, we have performed a full DMC calculation on the subject of  $^4\text{He}$  adsorbed in carbon nanotube bundles. We have found a low-density liquid phase characterized by a single helium layer close to the nanotube wall. When the density increases there is a phase transition to a two-layer arrangement that will eventually solidify with further increase of the number of adsorbed helium atoms. We also saw that the influence of the neighbouring tubes in a bundle in the properties of a given one is negligible. Experimental signatures of the phases predicted in this work could be obtained by means of low temperature specific heat measurements<sup>7</sup> and neutron diffraction<sup>6</sup>.

### Acknowledgments

We acknowledge partial financial support from the Spanish Ministry of Education and Science (MEC) (grants FIS2006-02356-FEDER and FIS2005-04181), Junta de Andalucia (group FQM-205) and Generalitat de Catalunya (grant 2005GR-00779).

<sup>1</sup> A.C. Dillon, K.M. Jones, T.A. Bekkedahl, C.H. Kiang, D.S. Bethune and M.J. Heben, *Nature (London)*, **386** 377 (1997).  
<sup>2</sup> S. Talapatra, A.Z. Zambano, S.E. Weber and A.D. Migone, *Phys. Rev. Lett.* **85** 138 (2000).  
<sup>3</sup> W. Teizer, R.B. Hallock, E. Dujardin and T.W. Ebbesen, *Phys. Rev. Lett.* **82** 5305 (1999).  
<sup>4</sup> T. Wilson, A. Tyburski, M.R. DePies, O.E. Vilches, D. Becquet and M. Bienfait. *J. Low Temp. Phys.* **126** 403 (2002).  
<sup>5</sup> S. Ramachandran, T.A. Wilson, D. Vandervelde, D.K. Holmes and O.E. Vilches. *J. Low Temp. Phys.* **134** 115 (2004).  
<sup>6</sup> J.V. Pearce, M.A. Adams, O.E. Vilches, M.R. Johnson and H.R. Glyde, *Phys. Rev. Lett.* **95** 185302 (2005).  
<sup>7</sup> J.C. Lasjaunias, K. Biljakovic, J.L. Sauvajol, P. Monceau, *Phys. Rev. Lett.* **91** 025901 (2003).  
<sup>8</sup> T. Wilson and O.E. Vilches. *Physica B*, **329-333** 278

(2003).  
<sup>9</sup> M.C. Gordillo. *Phys. Rev. Lett.* **96** 216102 (2006).  
<sup>10</sup> M.M. Calbi, M.W. Cole, S.M. Gatica, M.J. Bojan and G. Stan, *Rev. Mod. Phys.* **73** 857 (2001).  
<sup>11</sup> J. Boronat, M.C. Gordillo and J. Casulleras. *J. Low Temp. Phys.* **126** 199 (2002).  
<sup>12</sup> G. Stan, M.J. Bojan, S. Curtarolo, S.M. Gatica and M.W. Cole, *Phys. Rev. B*, **62** 2173 (2000).  
<sup>13</sup> M.C. Gordillo, J. Boronat and J. Casulleras. *Phys. Rev. B*, **61** R878 (2000).  
<sup>14</sup> E. Krotschek and M.D. Miller. *Phys. Rev. B*, **60** 13038 (1999).  
<sup>15</sup> L. Firlej and B. Kuchta. *Colloids and Surfaces A*. **241** 149 (2004).  
<sup>16</sup> M. Rossi, D.E. Galli and L. Reatto. *Phys. Rev. B*, **72** 064516 (2005).  
<sup>17</sup> M. Rossi, D.E. Galli and L. Reatto. *J. Low Temp. Phys.* **149** 95 (2007).

- <sup>18</sup> J. Boronat and J. Casulleras. Phys. Rev. B **49** 8920 (1994).
- <sup>19</sup> G. Stan and M.W. Cole, Surf. Sci. **395** 280 (1998).
- <sup>20</sup> R.A. Aziz, F.R.W McCourt and C.C. K. Wong. Mol. Phys. J. Chem. Phys. **61** 1487 (1987).
- <sup>21</sup> J. Hoffmann and P. Nielaba. Phys. Rev. E, **67** 036115 (2003).
- <sup>22</sup> J. Tersoff and R.S. Ruoff. Phys. Rev. Lett. **73** 676 (1994).
- <sup>23</sup> M.E. Pierce and E. Manousakis. Phys. Rev. Lett. **83** 5314 (1999).
- <sup>24</sup> M.C. Gordillo, J. Boronat and J. Casulleras. Phys. Rev. B, **65** 014503 (2001).
- <sup>25</sup> R.L. Elgin and D.L. Goodstein. Phys. Rev. A **9** 2657 (1974).